

# Turbulence structure in boundary layers over periodic two- and three-dimensional roughness

RALPH J. VOLINO<sup>1</sup>†, MICHAEL P. SCHULTZ<sup>2</sup> AND  
KAREN A. FLACK<sup>1</sup>

<sup>1</sup>Mechanical Engineering Department, United States Naval Academy, Annapolis, MD 21402, USA

<sup>2</sup>Naval Architecture and Ocean Engineering Department, United States Naval Academy,  
Annapolis, MD 21402, USA

(Received 1 September 2010; revised 14 January 2011; accepted 19 January 2011;  
first published online 15 March 2011)

Measurements are presented from turbulent boundary layers over periodic two- and three-dimensional roughness. Cases with transverse rows of staggered cubes and cases with solid square transverse bars of two sizes were considered. Previous results by Volino, Schultz & Flack (*J. Fluid Mech.* vol. 635, 2009, p. 75) showed outer-layer similarity between cases with three-dimensional roughness and smooth walls, and deviations from similarity in cases with large two-dimensional transverse bars. The present results show that differences also occur with small two-dimensional bars and to a lesser extent when the bars are replaced with rows of staggered cubes. Differences are most apparent in correlations of turbulence quantities, which are of larger spatial extent for the rough-wall cases. The results with the staggered cubes indicate that part of the periodic roughness effect is caused by the repeated disturbance and recovery of the boundary layer as it encounters a row of roughness followed by a smooth surface. A larger effect, however, is due to the blockage caused by the two-dimensional transverse bars, which extend across the entire width of the boundary layer. The small two-dimensional bars have a larger effect than the staggered cubes, in spite of the bar height being only 11 viscous units and 1/7 of the cube height. The effect of the small bars extends well into the outer flow, indicating that effects observed previously with larger bars were not due only to a thickening of the roughness sublayer. The observed differences between the rough- and smooth-wall results are believed to be caused by large-scale attached eddies which extend from the roughness elements to the edge of the boundary layer.

**Key words:** boundary layer structure, turbulent boundary layers

---

## 1. Introduction

Roughness plays an important role in many wall-bounded flows, as most surfaces of practical interest have texture or imperfections due to machining, fouling, pitting, surface deposits, etc. The surface roughness generally leads to significant increases in drag as the near-wall fluid moves around and over roughness elements. Even surfaces that demonstrate smooth behaviour at low velocities can show roughness effects with increasing Reynolds number. Understanding the mechanisms responsible for the changes in turbulence parameters and increase in drag for a wide range of

† Email address for correspondence: volino@usna.edu

roughness types is important for the prediction of aerodynamic and hydrodynamic performance.

A wide range of rough surfaces have been investigated as outlined in the review articles of Raupach, Antonia & Rajagopalan (1991), Jiménez (2004) and Flack & Schultz (2010). The focus of these studies has been to understand the extent that roughness modifies the turbulent boundary layer for frictional drag prediction and flow modelling. While geometric factors such as roughness height, slope and density are important, whether the roughness geometry is two-dimensional (2-D, e.g. transverse rods, bars) or three-dimensional (3-D) has proven to be particularly significant. An important modelling assumption is that the flow over the rough-wall boundary layer is similar to the flow over a smooth wall outside of a roughness sublayer. Townsend's (1976) Reynolds number similarity hypothesis states that turbulent motions in the outer flow are unaffected by surface conditions when normalized with the friction velocity,  $u_\tau$ , and the boundary layer thickness,  $\delta$ . The hypothesis assumes that  $\delta$  is large compared to the roughness height  $k$ . A number of studies have shown support for Townsend's hypothesis for 3-D roughness of various types including the works of Ligrani & Moffat (1986) for packed spheres, Perry & Li (1990) for expanded mesh, Flack, Schultz & Shapiro (2005) for sandpaper and mesh, Kunkel & Marusic (2006) for salt flats ground cover, Shockling, Allen & Smits (2006) for a honed pipe, Schultz & Flack (2007) for a scratched surface and Wu & Christensen (2007) for roughness replicating deposits on gas turbine blades. Similarity has also been observed to exist for large 3-D roughness as demonstrated by Castro (2007) for mesh, staggered cubes and gravel chips with  $k/\delta < 1/10$  for the largest roughness, and by Flack, Schultz & Connelly (2007) for mesh and sandpaper with  $k/\delta < 1/16$ . Similarity in the turbulence structure, as quantified by turbulence spectra, probability density functions (PDFs) of the swirl strength, two-point spatial correlations of turbulence quantities and swirl, structure angles and length scales of correlations, was reported by Volino, Schultz & Flack (2007) for mesh roughness. The dominant structure in both the rough-wall and smooth-wall outer layers was the vortex packet. Wu & Christensen (2007) reported similarity in the outer-layer turbulence structure for smooth walls and a wall with replicated turbine blade roughness.

While most studies have demonstrated that outer-layer similarity with smooth-wall boundary layers holds for a large range of 3-D roughness types and sizes, boundary layers over 2-D  $k$ -type roughness have exhibited different behaviour. Krogstad & Antonia (1999) considered 2-D transverse rods. The streamwise rod spacing,  $p$ , in this case was four times the rod diameter. Significant increases in the Reynolds stresses above smooth-wall results, particularly in the  $\overline{v'^2}^+$  and  $-\overline{u'v'}^+$  components, were present throughout the boundary layer. Leonardi *et al.* (2003) performed a direct numerical simulation (DNS) of flow over transverse bars on one wall of a channel with  $1.33 < p/k < 20$ . A bar spacing of  $p/k = 8$  resulted in the largest form drag and subsequently produced the largest roughness function. Djenidi *et al.* (2008) conducted experiments with 2-D transverse square bars and  $p/k$  ranging from 8 to 16. The roughness function was greatest for  $p/k = 8$ ; however, the largest effect on the Reynolds stresses occurred for  $p/k = 16$ . Volino, Schultz & Flack (2009) conducted experiments with transverse square bars and  $p/k = 8$ . They reported an increase in the Reynolds stresses in the outer layer for the 2-D bars compared to smooth-wall cases. They also noted the same hairpin structure as in smooth-wall cases with the same flow structure angles. Frequent eruptions of the fluid from the near-wall region were observed which extended into the outer part of the boundary layer over 2-D roughness. These eruptions were not observed over smooth walls or

walls with 3-D mesh roughness. The eruptions were tied to about a 40 % increase in the extent of attached eddies from the wall into the boundary layer. Two-point correlations of turbulence quantities and swirl strength indicated an increase in the size of flow structures in the 2-D roughness case by about 40 % in the streamwise and wall-normal directions, and 15 % in the spanwise direction compared to smooth-wall and 3-D roughness cases. Lee & Sung (2007) conducted a DNS for a turbulent boundary layer over a wall with 2-D disturbances. The disturbances modelled 2-D transverse square bars with  $p/k=8$ . They also reported an increase of all the Reynolds normal stresses and the Reynolds shear stress across most of the boundary layer. The aforementioned studies all involved turbulent boundary layers. Krogstad *et al.* (2005) considered a turbulent channel flow with 2-D bars both experimentally and with DNS, and for the most part showed no roughness effects in the outer layer. As noted in Krogstad *et al.* (2005) and also in Volino *et al.* (2009), channel flows respond differently to roughness than boundary layer flows possibly due to the difference in the outer boundary condition.

The studies discussed above seem to indicate that 2-D and 3-D roughnesses affect turbulent boundary layers differently. For these studies, the 2-D roughness height has been a significant fraction of the boundary layer thickness and the spacing of the 2-D elements has been such as to create a large disturbance. It is therefore unclear whether 2-D roughness behaves in a fundamentally different way than 3-D roughness or whether the differences observed are simply due to the relative roughness height or the manner in which the boundary layer is periodically disturbed. The aim of this paper is to experimentally investigate two fundamental questions, posed below, related to the differences observed between 2-D and 3-D rough-wall boundary layers.

First, does 2-D roughness cause a breakdown of Townsend's outer-layer similarity hypothesis, or does 2-D roughness simply increase the thickness of the roughness sublayer relative to the total boundary layer thickness? For 3-D roughness, Flack *et al.* (2007) found that the roughness sublayer extended roughly  $5k$  or  $3k_s$  from the wall, with  $5k$  approximately equal to  $3k_s$ . For 2-D  $k$ -type roughness,  $k_s$  can be much larger than  $k$ , as the flow must go over the top of 2-D transverse roughness elements, while for 3-D elements the flow can simply go around the roughness. When the flow goes over the top of a 2-D element, the boundary layer separates, and if  $p/k$  is sufficiently large, it reattaches before the next element. The repeated separating and reattaching results in a large effective roughness height relative to  $k$ . In the 2-D roughness case of Volino *et al.* (2009),  $k_s/k=13.6$ . Significant differences were seen between the 2-D rough- and smooth-wall cases outside of  $5k$ , but if the outer layer were defined in terms of  $3k_s$ , the entire boundary layer would be within the roughness sublayer, and no conclusion could be drawn regarding outer-layer similarity. Most of the previous studies that observed differences in the Reynolds stresses used 2-D roughness with a large effective roughness height. Outer-layer similarity may hold if the size of the 2-D roughness elements is significantly reduced.

A second question arises regarding the mechanism by which 2-D roughness changes the boundary layer. Are the differences observed between 2-D and 3-D roughness cases due to the 2-D nature of the roughness elements themselves, which completely block the near-wall flow, or is the repeated disturbance and recovery caused by elements with large  $p/k$  that is responsible for the changes in the boundary layer? If the latter is the case, then 3-D roughness elements in an arrangement that repeatedly disturb the boundary layer may produce outer-layer effects. Possibly both spanwise blockage and repeated disturbances play a role.

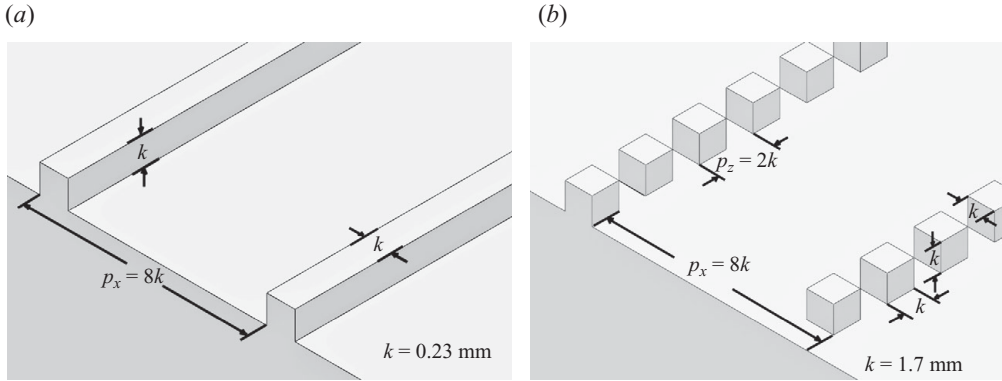


FIGURE 1. Schematic of (a) a 2-D bar and (b) 3-D staggered cube roughness.

The present study addresses the above questions. To test outer-layer similarity, a wall was fabricated with very small transverse bars. Comparisons will be made between the flows over the previously tested larger bars and the bars that have a roughness height 7.5 times smaller. The small-bars result in a boundary layer with  $\delta$  significantly larger than  $k_x$ . To answer the second question, experiments were conducted on a wall with the transverse bars of Volino *et al.* (2009) replaced by rows of staggered cubes with the same  $k$  and  $p/k$ . The boundary layer experiences repeated disturbances; however, the flow can move around the roughness elements through transverse gaps of dimension  $k$ . Comparisons will be made between the flow over the previously tested larger transverse bars and the rows of staggered cubes.

## 2. Experiments and data processing

Experiments were conducted in the water tunnel as described by Volino *et al.* (2007). The test section was 2 m long, 0.2 m wide and nominally 0.1 m tall. The lower wall was a flat plate which served as the test wall. The upper wall was adjustable and set for a zero streamwise pressure gradient. The acceleration parameter, defined as

$$K = \frac{v}{U_e^2} \frac{dU_e}{dx}, \quad (2.1)$$

was less than  $5 \times 10^{-9}$ . The upper wall and sidewalls provided optical access. The first test wall was an acrylic plate machined with small 2-D transverse square bars, as shown in figure 1. The bar height was  $k = 0.23 \text{ mm}$ . The bar spacing was  $p/k = 8$ . The second test wall was also an acrylic plate and was machined with rows of staggered cubes, as shown in figure 1. The cube height was  $k = 1.7 \text{ mm}$ . The spanwise spacing between the cubes was also 1.7 mm. The streamwise spacing between the rows was  $p/k = 8$ . For both test walls, the boundary layer was tripped near the leading edge with a 0.8 mm diameter wire, ensuring a turbulent boundary layer. Velocity measurements showed that a core flow remained at the measurement location. Smooth and large 2-D transverse bar comparison cases were documented in Volino *et al.* (2007) and Volino *et al.* (2009) respectively. An acrylic test plate was used for the smooth-wall case. The large 2-D bars were machined in a similar plate with bars of the same height and streamwise spacing as the cubes of the present study.

The present geometry was selected to maintain the same  $p/k$  (as defined in figure 1) for both of the present roughness types. Previous investigations have shown that the response of the flow is sensitive to this ratio (e.g. Perry, Schofield & Joubert 1969;

Wall	$x$ (m)	$U_e$ (m s <sup>-1</sup> )	$\delta$ (mm)	$u_\tau$ (m s <sup>-1</sup> )	$Re_\theta$ $U_e \theta / \nu$	$Re_\tau = \delta^+$ $= u_\tau \delta / \nu$	$k_s^+$ $= k_s u_\tau / \nu$	$k/\delta$
Small 2-D bars	1.00	0.951	36.7	0.0492	4984	1749	97	0.0062
3-D staggered cubes	1.00	0.681	46.9	0.0391	4952	1869	255	0.036
Smooth wall	1.50	1.255	35.2	0.0465	6069	1772	—	—
Large 2-D bars	1.00	0.499	54.6	0.0341	4260	1790	755	0.031

TABLE 1. Boundary layer parameters.

Furuya, Miyata & Fujita 1976). In maintaining  $p/k$ , the roughness area density ratio, defined as the windward frontal area of the roughness divided by the planform area, is 12.5 % for the 2-D bars and 6.25 % for the 3-D cubes. Leonardi & Castro (2010) showed that the area density ratio is an important parameter for arrays of staggered cubes and that the largest drag is produced for roughness area density ratios of  $\sim 15$  %. Although they do not match, both area ratios lie in what is considered the sparse roughness regime as defined by Jiménez (2004).

Flow was supplied to the test section from a 4000 l cylindrical tank. Water was drawn from the tank to two variable speed pumps operating in parallel and then sent to a flow conditioning section consisting of a diffuser containing perforated plates, a honeycomb, three screens and a 3-D contraction. The test section followed the contraction. The free-stream turbulence level was less than 0.5 %. Water exited the test section through a perforated plate emptying into the cylindrical tank. The test fluid was filtered and deaerated water. A chiller was used to keep the water temperature constant to within 1°C during all tests.

Boundary layer velocity measurements were obtained with a TSI FSA3500 two-component laser Doppler velocimeter (LDV). The LDV consists of a four-beam fibre optic probe that collects data in backscatter mode. A custom-designed beam displacer was added to the probe to shift one of the four beams, resulting in three co-planar beams that can be aligned parallel to the wall. Additionally, a 2.6:1 beam expander was located at the exit of the probe to reduce the size of the measurement volume. The resulting probe volume diameter ( $d$ ) was 45  $\mu\text{m}$  with a probe volume length ( $l$ ) of 340  $\mu\text{m}$ . The corresponding measurement volume diameter and length in viscous length scales were  $d^+ \leq 2.2$  and  $l^+ \leq 16$ .

Measurements were made 1 m downstream of the trip. The velocity in the test section was set for each case so that the turbulent Reynolds number approximately matched the value of the smooth-wall comparison case, as shown in table 1. For the velocity profiles, the LDV probe was traversed to 40 locations within the boundary layer with a Velmex three-axis traverse unit. The traverse allowed the position of the probe to be maintained to  $\pm 5 \mu\text{m}$  in all directions. A total of 50 000 random velocity samples were obtained at each location in the boundary layer. The data were collected in coincidence mode. The flow was seeded with 2  $\mu\text{m}$  diameter silver-coated glass spheres. The seed volume was controlled to achieve acceptable data rates while maintaining a low burst density signal (Adrian 1983). Measurements were made  $3k$  downstream of the centre of a roughness element. Measurements showed no significant variation between profiles acquired at different streamwise or spanwise positions except for a region within about  $3k$  of the wall.

Flow-field measurements were acquired using particle image velocimetry (PIV). A streamwise-wall-normal ( $xy$ ) plane was acquired at the spanwise centreline of the test section. The flow was seeded with 2  $\mu\text{m}$  diameter silver-coated glass spheres. The light

source was a Nd:YAG laser set for a 350 μs interval between pulses for each image pair in the small 2-D transverse bar case and to a 525 μs interval for the 3-D cube case. The fields of view were 90 mm × 67 mm and 107 mm × 80 mm, in the 2-D bar and 3-D cube cases respectively, extending from near the wall into the free stream in both cases. A CCD camera with a 1376 × 1024 pixel array was used. Image processing was done with TSI Insight 3G software. Velocity vectors were obtained using 16 pixel square windows with 50 % overlap. For each measurement plane, 2000 image pairs were acquired for processing.

The data processing techniques used to compute the mean velocity, turbulence statistics and wall shear are described in detail in Schultz & Flack (2007). The techniques used to compute spatial correlations and swirl strength are described in Volino *et al.* (2007) and defined again below.

The two-point spatial correlation is defined at the wall-normal position  $y_{ref}$  as

$$R_{AB}(y_{ref}) = \frac{\overline{A(x, y_{ref})B(x + \Delta x, y_{ref} + \Delta y)}}{\sigma_A(y_{ref})\sigma_B(y_{ref} + \Delta y)}, \quad (2.2)$$

where  $A$  and  $B$  are the quantities of interest at two locations separated in the streamwise and wall-normal directions by  $\Delta x$  and  $\Delta y$ , and  $\sigma_A$  and  $\sigma_B$  are the standard deviations of  $A$  and  $B$  at  $y_{ref}$  and  $y_{ref} + \Delta y$  respectively. At every  $y_{ref}$ , the overbar indicates that the correlations were averaged among location pairs with the same  $\Delta x$  and  $\Delta y$ , and then time averaged over the 2000 vector fields. Correlations of  $u$ ,  $v$ , the swirl strength, and all cross-correlations were considered.

The swirl strength,  $\lambda$ , can be used to locate vortices. It is closely related to the vorticity but discriminates between vorticity due only to shear and vorticity resulting from rotation. It is defined as the imaginary part of the complex eigenvalue of the local velocity gradient tensor and is defined as follows (Zhou *et al.* 1999):

$$[d_{ij}] = [v_r \ v_{cr} \ v_{ci}] \begin{bmatrix} \lambda_r & & \\ & \lambda_{cr} & \lambda_{ci} \\ & -\lambda_{ci} & \lambda_{cr} \end{bmatrix} [v_r \ v_{cr} \ v_{ci}]^{-1}, \quad (2.3)$$

where  $[d_{ij}]$  is the velocity gradient tensor. It is used in the present study in a 2-D form as explained in several studies including Hutchins, Hambleton & Marusic (2005). A more complete discussion is available in Chong, Perry & Cantwell (1990). By definition,  $\lambda$  is always  $\geq 0$ , but a sign can be assigned based on the local vorticity to show the direction of rotation. Rotation in the direction of the mean shear would have negative-signed swirl strength and is referred to as prograde swirl, and rotation in the opposite direction is referred to as retrograde. The swirl strength,  $\lambda$ , is assumed signed in the present work. In the  $xy$  plane,  $\lambda$  can be used to identify the heads of hairpin vortices.

### 3. Results

The boundary layer thickness, friction velocity and other quantities from the velocity profiles of the present cases and the comparison cases are presented in table 1. Although alone they do not necessarily guarantee fully rough conditions, the roughness Reynolds numbers based on the equivalent sand roughness height,  $k_s^+ = k_s u_\tau / \nu$ , which are 255 (cubes), 97 (small bars) and 755 (large bars) are large enough to imply fully rough conditions. The roughness Reynolds number is given by the following (Schlichting 1979):

$$\Delta U^+ = \frac{1}{\kappa} \ln k_s^+ - 3.5, \quad (3.1)$$

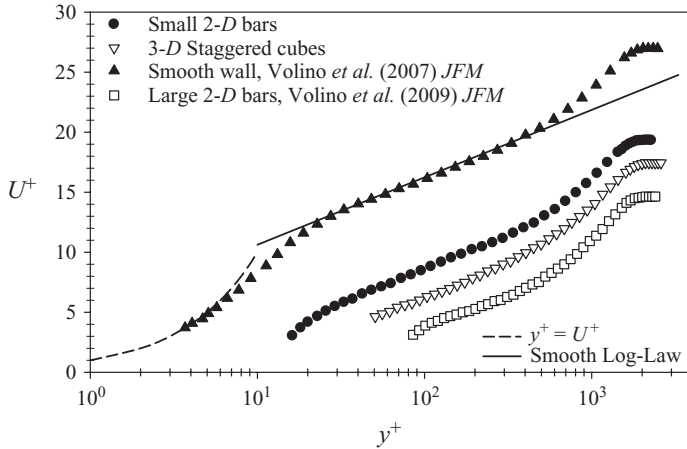


FIGURE 2. Mean velocity profiles in inner variables.

where  $\Delta U^+$  is the roughness function. The ratios of  $k_s/k$  are 13.6, 8.9 and 3.8 for the large bars, small bars and staggered cubes, respectively. These ratios agree with the results of Jiménez (2004), who showed  $k_s/k$  as a function of the blockage caused by roughness elements. Both  $k_s$  and  $k_s^+$  for the staggered cubes lie between the values for the two bar cases. The friction velocity,  $u_\tau$ , was determined using the Clauser chart method with  $\kappa = 0.41$  and  $B = 5.0$ . The uncertainty in  $u_\tau$  was  $\pm 3\%$  and  $\pm 6\%$  for the smooth- and rough-wall cases respectively. The total stress method was also used to evaluate  $u_\tau$ , and the resulting values agreed with those from the Clauser chart method to within 2%. The uncertainties in the boundary layer thickness (based here on  $U/U_e = 0.99$ ) and momentum thickness were 7% and 4% respectively.

Uncertainty estimates were obtained using the method of Moffat (1988) to combine precision and bias errors. Precision errors were found by using the observed variability from repeated velocity profiles taken on both the smooth and rough plates. The precision uncertainty bounds were calculated at 95% confidence. The LDV data were corrected for velocity bias using the burst transit time weighting scheme of Buchhave, George & Lumley (1979). Velocity gradient bias was corrected on the smooth-wall results using the methodology of Durst *et al.* (1998). Velocity gradient bias for the rough-wall profiles was insignificant due to the lack of velocity measurements very near the wall. Fringe bias was also considered insignificant, as the beams were shifted well above a burst frequency representative of twice the free-stream velocity (Edwards 1987). Further details of the uncertainty determination methods are given in Flack *et al.* (2005).

### 3.1. Mean velocity and turbulence profiles

Mean velocity profiles for the cases in table 1 are shown in figure 2 in inner coordinates. The results in figures 2 and 3 are based on LDV measurements. The larger roughness elements (both cubes and 2-D bars) result in a larger shift than the small bars, and the large bars result in a larger shift than the equally sized cubes. Mean velocity and Reynolds stress profiles are shown in outer coordinates in figure 3. As previously shown in Volino *et al.* (2009) for the smooth-wall and large 2-D bar cases, no clear differences are visible in the mean profiles in defect coordinates. Similarity in the mean profiles was also noted by Krogstad & Antonia (1999) for 2-D and 3-D roughnesses. These results indicate that the mean flow in the outer layer is fairly

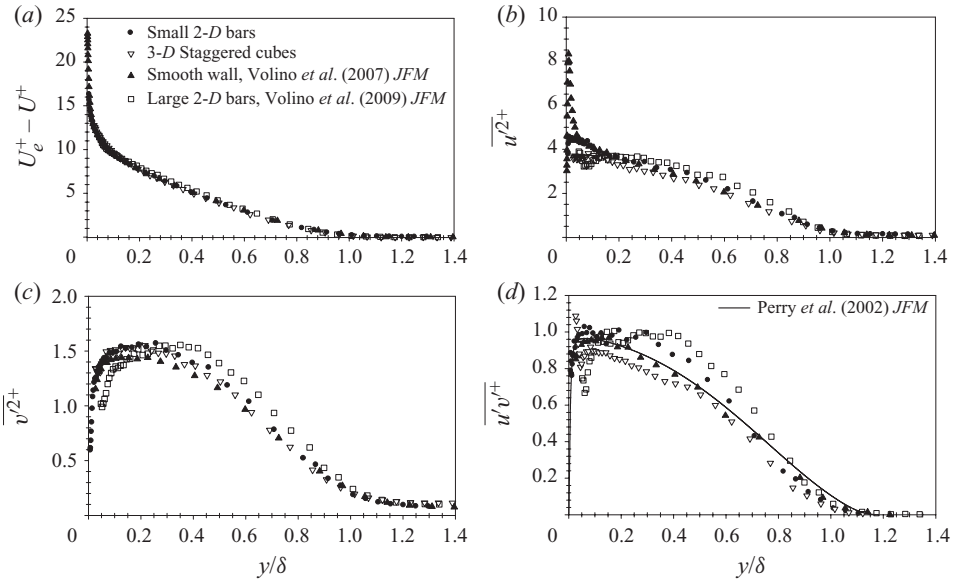


FIGURE 3. Velocity profiles in outer coordinates. (a) Mean velocity in defect form, (b) streamwise Reynolds normal stress, (c) wall-normal Reynolds normal stress and (d) Reynolds shear stress.

insensitive to surface conditions, even for significant wall perturbations, consistent with the observations of Connelly, Schultz & Flack (2006) and Castro (2007).

The  $\overline{u'^2}^+$  normal stress is shown in figure 3(b). The results for the large 2-D bars are somewhat higher than those in the smooth-wall case in the outer layer, but the differences are not large. No significant effect is observed for the small 2-D bars or the 3-D cubes outside the roughness sublayer. The present observation that surface roughness has little effect on  $\overline{u'^2}^+$  in the outer flow is consistent with the literature (e.g. Krogstad & Antonia 1999; Flack *et al.* 2005; Wu & Christensen 2007).

The  $\overline{v'^2}^+$  normal stress is presented in figure 3(c). The large 2-D roughness results are  $\sim 20\%$  higher than those in the smooth-wall case. This difference is observed to  $y/\delta$  of about 0.7. While  $\overline{v'^2}^+$  for both the small 2-D bars and the 3-D cubes lies above that in the smooth-wall case in the outer layer, the difference observed is much smaller than that for the large 2-D bar case. An increase in  $\overline{v'^2}^+$  for 2-D roughness is consistent with the observation of Krogstad & Antonia (1999).

For the  $-\overline{u'v'}^+$  profiles (figure 3d), differences between the four cases are more apparent. Again the large 2-D bars show the largest difference from the smooth wall, but the small bars show fairly large deviation as well, that persists for  $y/\delta < 0.7$ . For the small bars,  $y/\delta = 0.7$  corresponds to  $12.4k_s$ , indicating significant effects well beyond the roughness sublayer. Also shown for comparison is the analytical result from Perry, Marusic & Jones (2002), which agrees well with the present smooth-wall data. The results for the 3D cube are slightly below the smooth-wall results although this difference is within the experimental uncertainty of the measurements.

In all the Reynolds stresses the 3-D cube case shows a relatively small deviation from the smooth-wall results, while the 2-D bars exhibit larger differences, particularly in  $-\overline{u'v'}^+$ . This occurs despite the cubes being 7.5 and 3.2 times larger than the small bars in terms of  $k$  and  $k_s$ , respectively. In fact, the height of the small bars is only 11 viscous length scales. It appears, therefore, that 2-D roughness, even if very small, can

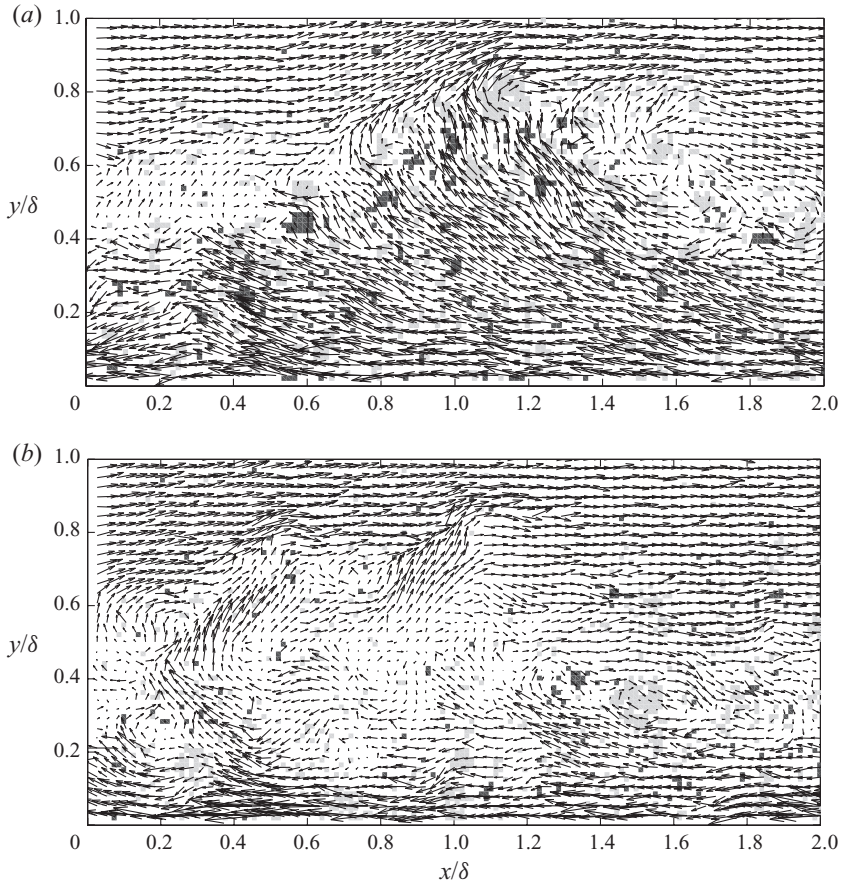


FIGURE 4. Instantaneous velocity vector field realizations with prograde swirl (grey shading) and retrograde swirl (black shading) superimposed: (a) small 2-D bars and (b) 3-D cubes.

give rise to significant changes in the outer flow. This is noteworthy given that such changes are not observed for most types of 3-D roughness, even in the limit of large roughness height (e.g. Flack *et al.* 2007). In comparing the present Reynolds stress results for the small 2-D bars and 3-D cubes, the spanwise blockage caused by the 2-D bars appears to have a larger effect than the repeated disturbance and recovery of the boundary layer that results from roughness with streamwise periodicity. In the following section, the turbulence structure for each of the cases will be considered.

### 3.2. Velocity fields, $xy$ plane

Instantaneous velocity vector fields shown in Volino *et al.* (2009) showed frequent large eruptions of fluid which extended from the near-wall region to the edge of the boundary layer in the large 2-D bar case. Such eruptions were not seen in the smooth-wall case or in 3-D roughness cases considered. In the present study, the large eruptions were witnessed for all the rough-surface cases. Instantaneous realizations are shown in figure 4 for the present rough-wall cases with a uniform convection velocity  $0.8U_e$  subtracted from each field. It should be noted that while large eruptions were observed for both the small 2-D bar and 3-D cube cases, they were more routinely observed and typically stronger for the small bars than for the cubes. This difference in structure is quantified in figure 5, which shows the PDF of the instantaneous Reynolds

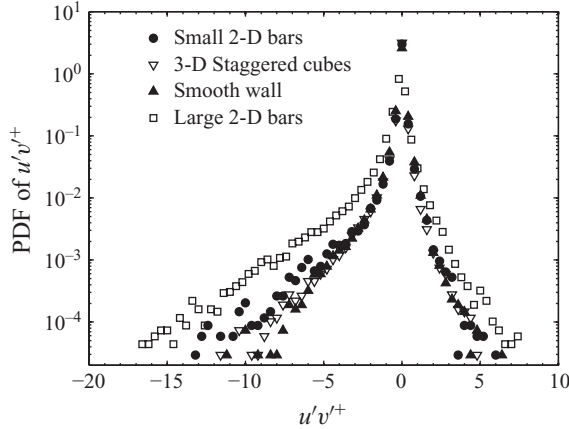


FIGURE 5. Probability density function of instantaneous  $u'v'^+$  at  $y/\delta = 0.8$ .

shear stress ( $u'v'^+$ ) for  $y/\delta = 0.8$ . Very strong  $-u'v'^+$  events are much more prevalent for the 2-D roughness cases than for the smooth-wall case. Events at  $y/\delta = 0.8$  with  $-u'v'^+ < -4$  occur 2.0 times as often with the small 2-D bars than with the smooth wall, and 6.8 times as often with the large 2-D bars than with the smooth wall. A more modest increase is observed for the 3-D staggered cubes, which show a 7% rise in events with  $-u'v'^+ < -4$  than in the smooth-wall case.

Further quantification of the flow structure is provided in figure 6, which shows two-point correlations of the streamwise fluctuating velocity,  $R_{uu}$ , with the correlation centred at  $y_{ref}/\delta = 0.4$ . The contours in figures 6(a) and 6(d) have similar shape, but the small and large 2-D bars have the largest streamwise and wall-normal extent of  $R_{uu}$ . The 3-D cubes also show an increase in the spatial extent of  $R_{uu}$  compared to the smooth wall, although the increase is not as large as that observed for the 2-D cases. The angle of inclination of  $R_{uu}$  is related to the average inclination of the hairpin packets. It was determined, as in Volino *et al.* (2007), using a least-squares method to fit a line through the points farthest from the self-correlation peak on each of the five  $R_{uu}$  contour levels 0.5, 0.6, 0.7, 0.8 and 0.9 both upstream and downstream of the self-correlation peak. For the present cases, the inclination angle remains nearly constant for reference points between  $y/\delta = 0.2$  and 0.5. For  $y/\delta < 0.2$  the angle drops somewhat as the contours begin to merge with the wall. For  $y/\delta > 0.5$ , the angle decreases towards zero, as these points tend to be above the hairpin packets which produce the inclination. For  $0.2 < y/\delta < 0.5$ , the angles are  $12.0^\circ \pm 1.3^\circ$ ,  $13.2^\circ \pm 1.4^\circ$ ,  $10.2^\circ \pm 2.7^\circ$  and  $10.6^\circ \pm 1.2^\circ$  for the small 2-D bars, 3-D cubes, smooth and large 2-D bar cases respectively. The range in each case indicates the span about the average observed between  $y/\delta = 0.2$  and 0.5. The difference between the cases is comparable to the scatter in the data and the range reported in the literature for smooth-wall boundary layers (e.g. Adrian, Meinhardt & Tomkins 2000). Therefore the large-scale events noted above do not significantly affect the structure angle.

The streamwise and wall-normal extents of  $R_{uu}$  are shown in figures 6(e) and 6(f) as a function of the reference point. The distance,  $Lx_{uu}$ , is defined as in Christensen & Wu (2005) as twice the distance from the self-correlation peak to the most downstream location on the  $R_{uu} = 0.5$  contour. In the streamwise direction, averaging between  $y/\delta = 0.2$  and 0.5, the 3-D cube results are 18% higher than the smooth-wall results. The small and large 2-D bar results are 26% and 38% higher respectively than

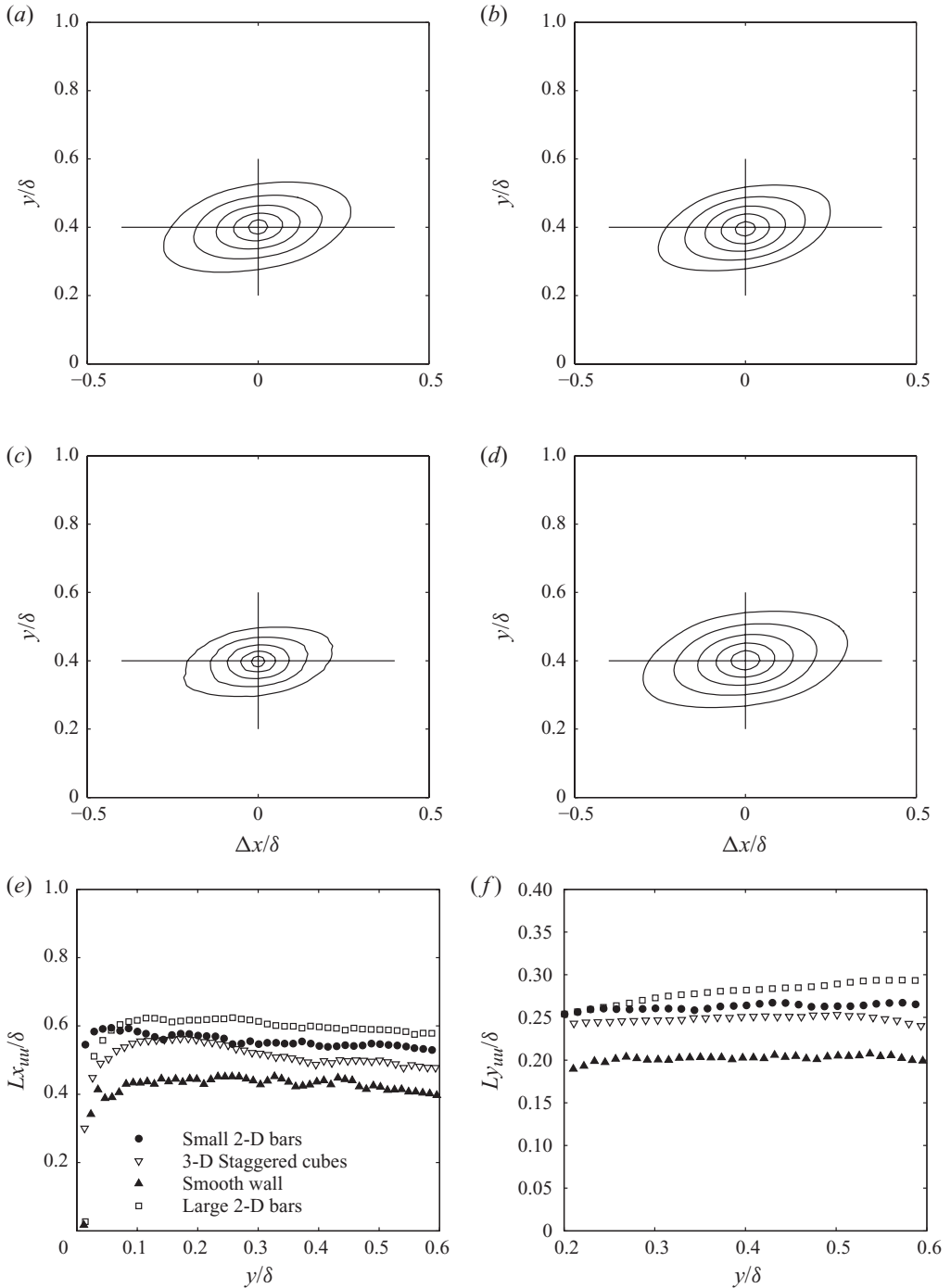


FIGURE 6. Contours of  $R_{uu}$  centred at  $y/\delta \approx 0.4$ , outermost contour  $R_{uu} = 0.5$ , contour spacing 0.1, (a) small 2-D bars, (b) 3-D staggered cubes, (c) smooth wall, (d) large 2-D bars; (e) streamwise extent of  $R_{uu} = 0.5$  contour as a function of  $y/\delta$  and (f) wall-normal extent of  $R_{uu} = 0.5$  contour as a function of  $y/\delta$ .

the smooth-wall results for the same  $y/\delta$  range. The wall-normal extent of the  $R_{uu}$  correlation,  $L_{y_{uu}}$ , is determined based on the wall-normal distance between the points closest and farthest from the wall on a particular contour. Figure 6(f) shows  $L_{y_{uu}}/\delta$  as a function of  $y/\delta$  using the  $R_{uu}=0.5$  contour. Due to the contours merging with the wall,  $L_{y_{uu}}$  drops towards zero for  $y/\delta < 0.2$ . Averaging between  $y/\delta=0.2$  and 0.5, the 3-D cubes result in 23 % larger  $L_{y_{uu}}$  than the smooth wall, while the small and large 2-D bars result in 30 % and 37 % larger lengths than the smooth wall respectively. These results are consistent with the Reynolds stresses in figure 3, which show that 2-D bars, particularly the large bars, have more effect than the 3-D cubes.

Figure 7 shows  $R_{vv}$  contours centred at  $y/\delta=0.4$  along with  $L_{x_{vv}}$  and  $L_{y_{vv}}$  as functions of  $y/\delta$ . The length  $L_{x_{vv}}$  is determined based on the streamwise distance between the most upstream and downstream points on the  $R_{vv}=0.5$  contour. The length  $L_{y_{vv}}$  is defined as above for the  $R_{uu}$  results. The streamwise extent of  $R_{vv}$  is considerably less than that of  $R_{uu}$ , since  $R_{uu}$  is tied to the common convection velocity of each hairpin packet. The ratio  $L_{x_{vv}}/L_{y_{vv}}$  is about 0.75 for all walls. The streamwise and wall-normal length scales average 35 % and 29 % larger for  $L_{x_{vv}}$  and  $L_{y_{vv}}$  respectively for the large 2-D bars compared to the smooth wall. The 3-D cube and small 2-D bars results are approximately equal and lie between the smooth-wall and large-bar results at about 18 % and 13 % above the smooth wall for  $L_{x_{vv}}$  and  $L_{y_{vv}}$  respectively.

Contours of the cross-correlation  $R_{uv}$  centred at  $y/\delta=0.4$  are shown in figure 8 along with  $L_{x_{uv}}$  and  $L_{y_{uv}}$  as functions of  $y/\delta$ . The lengths are computed as for  $R_{vv}$  but are based on the  $-0.15$  contour. As with  $R_{uu}$  and  $R_{vv}$ , the general shape of the correlation contours is the same for all walls. For the 3-D cubes,  $L_{x_{uv}}$  and  $L_{y_{uv}}$  are 16 % and 19 % larger respectively than in the smooth-wall case. The small 2-D bar results are about 30 % larger than the smooth-wall results in both directions. The large 2-D bar results are 34 % and 41 % above the smooth-wall values for  $L_{x_{uv}}$  and  $L_{y_{uv}}$  respectively.

Contours of the auto-correlation of the signed swirl strength,  $R_{\lambda\lambda}$ , at  $y/\delta=0.4$  are shown in figure 9 along with  $L_{x_{\lambda\lambda}}$  and  $L_{y_{\lambda\lambda}}$ , which are based on the  $R_{\lambda\lambda}=0.5$  contour. The 3-D cube and smooth-wall results are close to each other with the 3-D cube values slightly lower. As with the other correlations, the spatial extent is larger in the large 2-D bar case, by an average of 56 % in  $L_{x_{\lambda\lambda}}$  and 58 % in  $L_{y_{\lambda\lambda}}$  compared to the smooth wall. The small 2-D bar results lie between the large 2-D bar and smooth-wall results at about 20 % above the smooth-wall values.

In summary, the shapes of the two-point correlations are similar for all four walls, but the spatial extent of the correlations varies between walls. Differences between the 3-D cube and smooth-wall results are small for the  $R_{\lambda\lambda}$  correlation, but the extents of the 3-D cube correlations average 18 % larger than the smooth-wall results for the Reynolds stresses. The 2-D bars cause more variation, with the small bars resulting in roughly a 25 % increase in the length scales over smooth-wall values for all quantities including  $R_{\lambda\lambda}$  and the large bars resulting in about a 40 % increase over the smooth wall. This is consistent with the presence of the large-scale motions noted above for the rough-wall cases, and potentially a result of repeated separation and reattachment of the boundary layer.

The above results show a clear difference between flows over smooth walls and walls with periodic roughness, possibly due to the large-scale ejections into the outer boundary layer caused by periodic roughness. Since the large structures are believed to originate at the roughness elements, they indicate a direct connection of the outer flow to the wall. They would be attached eddies in the terminology of Perry &

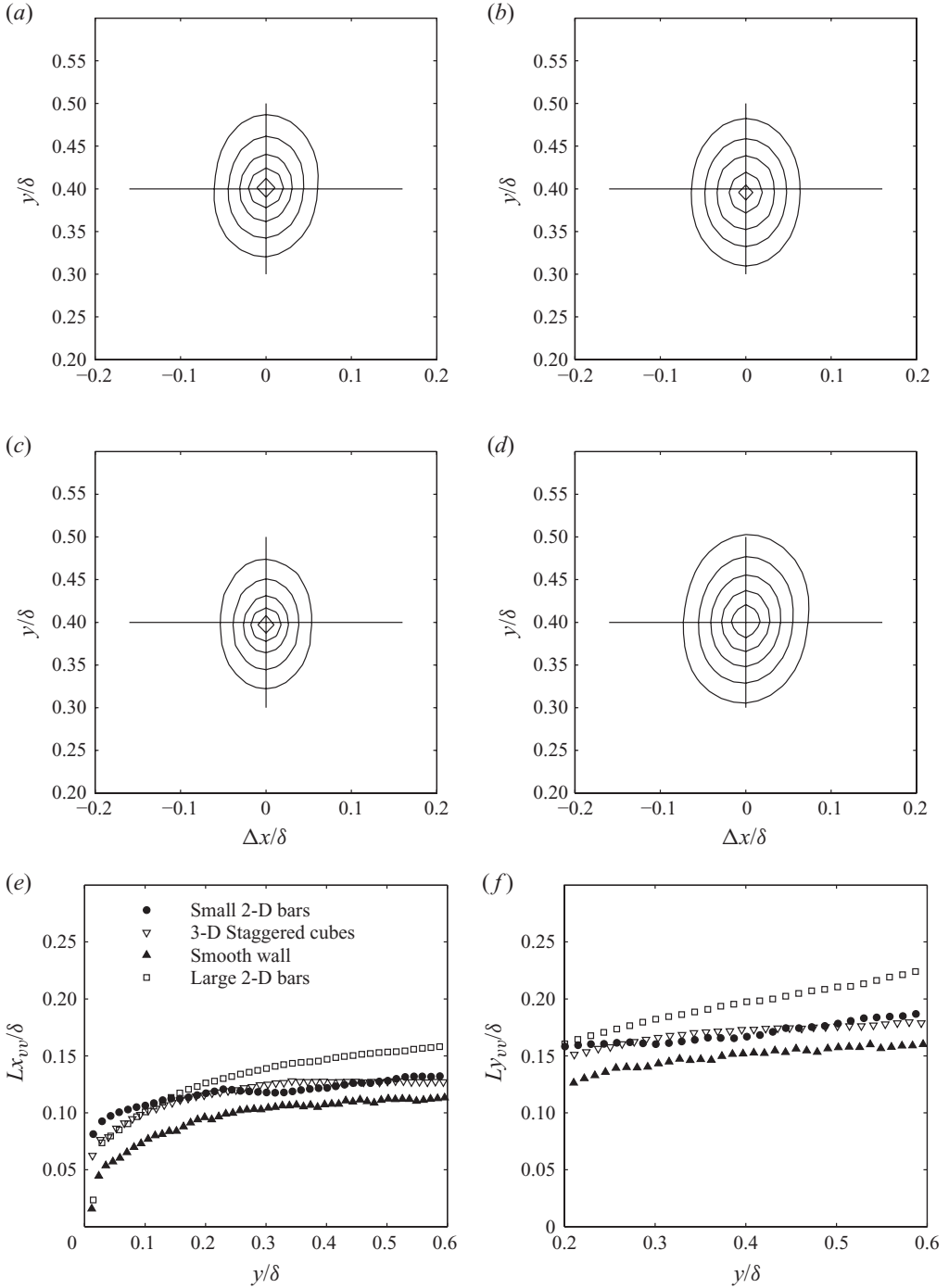


FIGURE 7. Contours of  $R_{vv}$  centred at  $y/\delta \approx 0.4$ , outermost contour  $R_{vv} = 0.5$ , contour spacing 0.1, (a) small 2-D bars, (b) 3-D staggered cubes, (c) smooth wall, (d) large 2-D bars; (e) streamwise extent of  $R_{vv} = 0.5$  contour as a function of  $y/\delta$  and (f) wall-normal extent of  $R_{vv} = 0.5$  contour as a function of  $y/\delta$ .

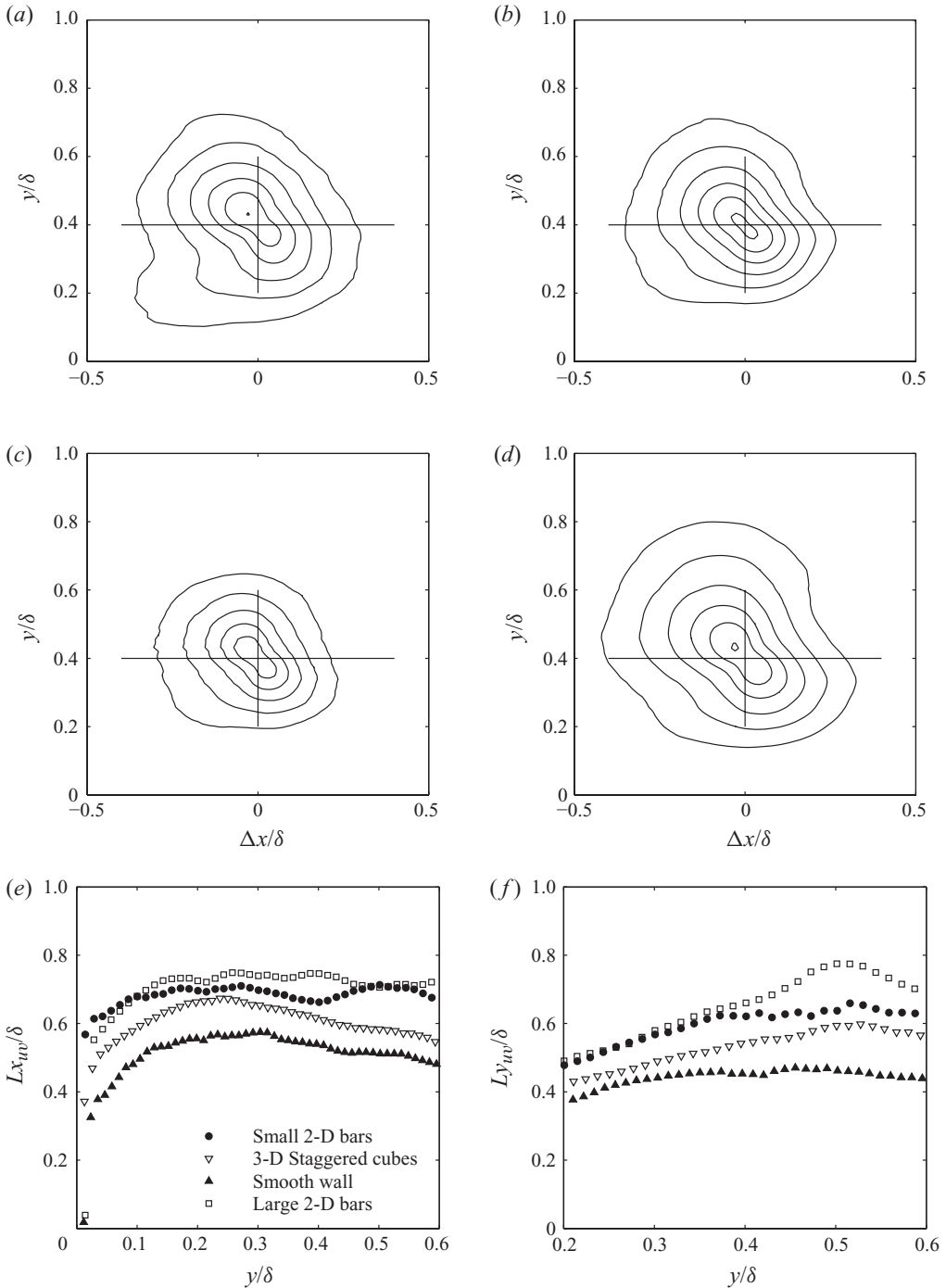


FIGURE 8. Contours of  $R_{uv}$  centred at  $y/\delta \approx 0.4$ , outermost contour  $R_{uv} = -0.15$ , contour spacing  $-0.05$ , (a) small 2-D bars, (b) 3-D staggered cubes, (c) smooth wall, (d) large 2-D bars; (e) streamwise extent of  $R_{uv} = -0.15$  contour as a function of  $y/\delta$  and (f) wall-normal extent of  $R_{uv} = -0.15$  contour as a function of  $y/\delta$ .

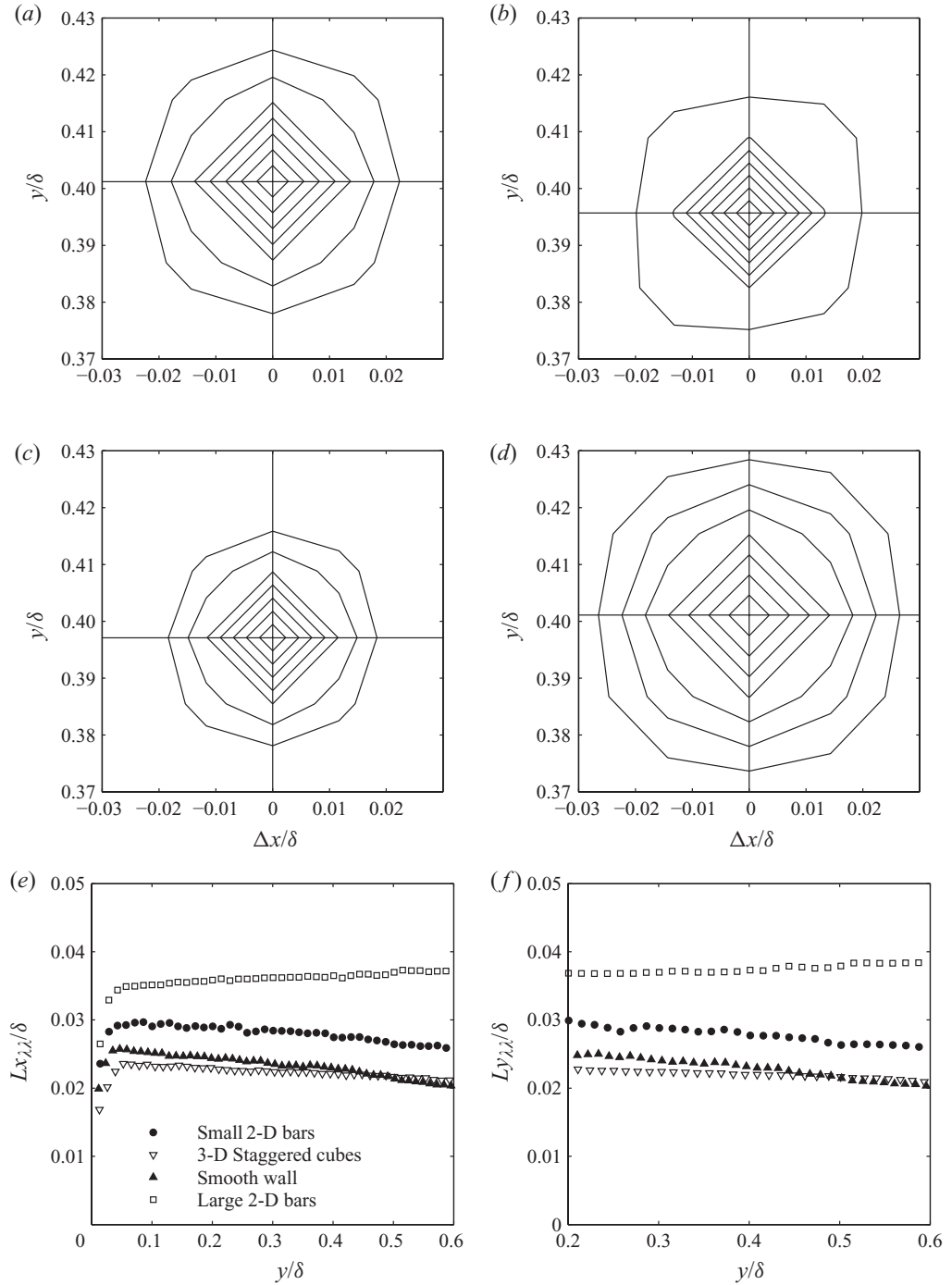


FIGURE 9. Contours of  $R_{\lambda\lambda}$  centred at  $y/\delta \approx 0.4$ , outermost contour  $R_{\lambda\lambda} = 0.3$ , contour spacing 0.1, (a) small 2-D bars, (b) 3-D staggered cubes, (c) smooth wall, (d) large 2-D bars; (e) streamwise extent of  $R_{\lambda\lambda} = 0.5$  contour as a function of  $y/\delta$  and (f) wall-normal extent of  $R_{\lambda\lambda} = 0.5$  contour as a function of  $y/\delta$ .

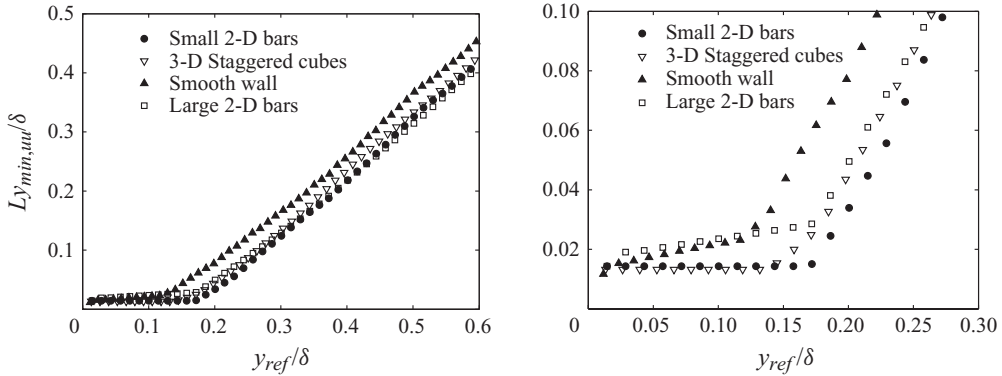


FIGURE 10. Distance from the wall to the closest point on  $R_{uu}=0.4$  contour,  $Ly_{min,uu}$ , as a function of the reference point for the contour, with an expanded view of slope transition on right.

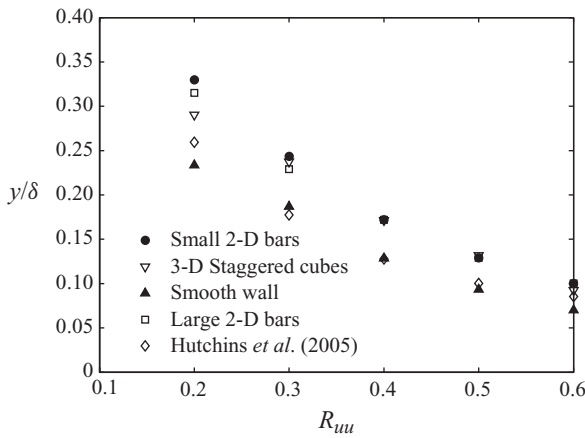


FIGURE 11. Location of slope change in  $Ly_{min,uu}$  (as in figure 10) as a function of  $R_{uu}$ .

Chong (1982). In the smooth-wall case, the outer part of the boundary layer contains only detached eddies (Perry & Marusic 1995), which have separated from the wall. Hutchins *et al.* (2005) used a plot of  $Ly_{min,uu}/\delta$  versus  $y_{ref}/\delta$ , where  $Ly_{min,uu}$  is the distance from the wall to the closest point on a particular  $R_{uu}$  contour and  $y_{ref}$  is the reference point for the contour, to quantify the distance that attached eddies extended into the boundary layer. For the  $R_{uu}=0.4$  contour used in figure 10, a change in the slope of  $Ly_{min,uu}$  is clear at  $y_{ref}/\delta=0.11$  for the smooth case, at  $y_{ref}/\delta=0.17$  for both 2-D bar cases and slightly lower at  $y_{ref}/\delta=0.15$  for the 3-D cube case. The change in slope is an indicator of the demarcation between attached and detached eddies. Its location depends on the choice of  $R_{uu}$  contour. Following the example of Hutchins *et al.* (2005), the demarcation is shown as a function of  $R_{uu}$  in figure 11. The smooth-wall results agree with the results of Hutchins *et al.* (2005). Attached eddies extend roughly 40% farther into the boundary layer for the rough-wall cases. If the detached eddies are similar in all turbulent boundary layers while the attached eddies depend on the wall condition, the extent of the attached eddies into the outer flow could explain the differences observed above for the rough-wall cases. Note that such differences and the large-scale ejections which are believed to cause them appear

to be peculiar to roughness which is periodically spaced in the streamwise direction. They are not observed for cases with 3-D roughness that is uniformly distributed in the streamwise direction (Volino *et al.* 2009).

#### 4. Conclusions

An experimental study has been carried out in a turbulent boundary layer over periodic two- and three-dimensional roughnesses. Included were cases with transverse rows of staggered cubes and cases with solid square transverse bars of two sizes. Previous results had shown outer-layer similarity between cases with three-dimensional roughness and smooth walls, and differences in cases with large 2-D transverse bars (Volino *et al.* 2009). The Reynolds stresses, particularly  $\overline{v'^2}^+$  and  $-\overline{u'v'}^+$ , increased in the outer part of the boundary layer with the 2-D bars compared to the smooth-wall case. The mean flow was not as significantly affected. Correlations of turbulence quantities indicated larger flow structures. The observed differences were caused by large-scale attached eddies which extend from the roughness elements to the edge of the boundary layer. The previous results raised the questions of whether these differences were due to changes in the outer layer or to a thickening of the roughness sublayer, and whether the effect was caused by the spanwise blockage caused by the 2-D bars or by their periodic streamwise spacing. The present results show that the differences are not simply due to a thickening of the roughness sublayer. The small 2-D bars tested had a height of only 11 viscous units, and the roughness sublayer (defined here as  $3k_s$ ) was within the inner 20 % of the boundary layer. Clear differences between the small-bar and smooth-wall results were observed outside the roughness sublayer, indicating that 2-D roughness does affect the flow structure in the outer layer. The outer-layer effects were apparent to some extent in the Reynolds stress profiles, particularly in  $-\overline{u'v'}^+$ , and were more apparent in spatial correlations of the turbulence, where increases in length scales of 25 % over smooth-wall results were observed. Results with the staggered 3-D cubes indicate that periodic disturbance and recovery of the boundary layer plays some role in changing the outer layer, with the same evidence of attached eddies extending into the outer flow as in the 2-D bar cases. Differences between the 3-D cube and smooth-wall results were small for the Reynolds stresses, but length scales of spatial correlations were about 18 % larger for the staggered cube case. The periodic disturbance alone, however, does not appear to have as large an effect as the blockage caused by 2-D transverse bars. Since the bars extend across the entire width of the boundary layer, the flow must go up and over them. In contrast it is possible for the flow to go around the sides of individual cubes. The large bars had a much larger effect than the cubes of equal size, and the small 2-D bars had a larger effect than the cubes, in spite of the small-bar height being only 1/7 of the cube height and  $k_s/\delta$  for the small bars being only 0.4 times the value for the cubes.

The authors would like to thank the Office of Naval Research for providing financial support under grants N00014-08-WR-2-0081 and N00014-08-WR-2-0159, and the United States Naval Academy Hydromechanics Laboratory for providing technical support.

#### REFERENCES

- ADRIAN, R. J. 1983 Laser velocimetry. In *Fluid Mechanics Measurements* (ed. R. J. Goldstein). Hemisphere.

- ADRIAN, R. J., MEINHART, C. D. & TOMKINS, C. D. 2000 Vortex organization in the outer region of the turbulent boundary layer. *J. Fluid Mech.* **422**, 1–54.
- BUCHHAVE, P., GEORGE, W. K. & LUMLEY, J. L. 1979 The measurement of turbulence with the laser-Doppler anemometer. *Annu. Rev. Fluid Mech.* **11**, 443–503.
- CASTRO, I. P. 2007 Rough-wall boundary layers: mean flow universality. *J. Fluid Mech.* **585**, 469–485.
- CHONG, M. S., PERRY, A. E. & CANTWELL, B. J. 1990 A general classification of 3-dimensional flow-fields. *Phys. Fluids A: Fluid Dyn.* **2**, 765–777.
- CHRISTENSEN, K. T. & WU, Y. 2005 Characteristics of vortex organization in the outer layer of wall turbulence. In *Proceedings of Fourth International Symposium on Turbulence and Shear Flow Phenomena, Williamsburg, VA*, vol. 3, pp. 1025–1030.
- CONNELLY, J. S., SCHULTZ, M. P. & FLACK, K. A. 2006 Velocity-defect scaling for turbulent boundary layers with a range of relative roughness. *Exp. Fluids* **40**, 188–195.
- DJENIDI, L., ANTONIA, R. A., AMIELH, M. & ANSELMET, F. 2008 A turbulent boundary layer over a two-dimensional rough wall. *Exp. Fluids* **44**, 37–47.
- DURST, F., FISCHER, M., JOVANOVIC, J. & KIKURA, H. 1998 Methods to set up and investigate low Reynolds number, fully developed turbulent plane channel flows. *Trans. ASME I: J. Fluids Engng* **120**, 496–503.
- EDWARDS, R. V. 1987 Report of the special panel on statistical particle bias problems in laser anemometry. *Trans. ASME I: J. Fluids Engng* **109**, 89–93.
- FLACK, K. A. & SCHULTZ, M. P. 2010 Review of hydraulic roughness scales in the fully rough regime. *J. Fluids Engng* **132**, 041203.
- FLACK, K. A., SCHULTZ, M. P. & CONNELLY, J. S. 2007 Examination of a critical roughness height for boundary layer similarity. *Phys. Fluids* **19**, 095104.
- FLACK, K. A., SCHULTZ, M. P. & SHAPIRO, T. A. 2005 Experimental support for Townsend's Reynolds number similarity hypothesis on rough walls. *Phys. Fluids* **17**, 035102.
- FURUYA, Y., MIYATA, M. & FUJITA, H. 1976 Turbulent boundary layer and flow resistance on plates roughened by wires. *Trans. ASME I: J. Fluids Engng* **98**, 635–644.
- HUTCHINS, N., HAMBLETON, W. T. & MARUSIC, I. 2005 Inclined cross-stream stereo particle image velocimetry measurements in turbulent boundary layers. *J. Fluid Mech.* **541**, 21–54.
- JIMÉNEZ, J. 2004 Turbulent flows over rough walls. *Annu. Rev. Fluid Mech.* **36**, 173–196.
- KROGSTAD, P.-Å., ANDERSSON, H. I., BAKKEN, O. M. & ASHRAFIAN, A. 2005 An experimental and numerical study of channel flow with rough walls. *J. Fluid Mech.* **530**, 327–352.
- KROGSTAD, P.-Å. & ANTONIA, R. A. 1999 Surface roughness effects in turbulent boundary layers. *Exp. Fluids* **27**, 450–460.
- KUNKEL, G. J. & MARUSIC, I. 2006 Study of the near-wall-turbulent region of the high-Reynolds-number boundary layer using an atmospheric flow. *J. Fluid Mech.* **548**, 375–402.
- LEE, S. H. & SUNG, H. J. 2007 Direct numerical simulation of the turbulent boundary layer over a rod-roughened wall. *J. Fluid Mech.* **584**, 125–146.
- LEONARDI, S., CASTRO & I. P. 2010 Channel flow over large cube roughness: a direct numerical simulation. *J. Fluid Mech.* **651**, 519–539.
- LEONARDI, S., ORLANDI, P., SMALLEY, R. J., DJENIDI, L. & ANTONIA, R. A. 2003 Direct numerical simulation of turbulent channel flow with transverse bars on one wall. *J. Fluid Mech.* **491**, 229–238.
- LIGRANI, P. M. & MOFFAT, R. J. 1986 Structure of transitionally rough and fully rough turbulent boundary layers. *J. Fluid Mech.* **162**, 69–98.
- MOFFAT, R. J. 1988 Describing the uncertainties in experimental results. *Exp. Therm. Fluid Sci.* **1**, 3–17.
- PERRY, A. E. & CHONG, M. S. 1982 On the mechanism of wall turbulence. *J. Fluid Mech.* **119**, 173–217.
- PERRY, A. E. & LI, J. D. 1990 Experimental support for the attached-eddy hypothesis in zero-pressure-gradient turbulent boundary layers. *J. Fluid Mech.* **218**, 405–438.
- PERRY, A. E. & MARUSIC, I. 1995 A wall-wake model for the turbulence structure of boundary layers. Part 1. Extension of the attached eddy hypothesis. *J. Fluid Mech.* **298**, 361–388.
- PERRY, A. E., MARUSIC, I. & JONES, M. B. 2002 On the streamwise evolution of turbulent boundary layers in arbitrary pressure gradients. *J. Fluid Mech.* **461**, 61–91.
- PERRY, A. E., SCHOFIELD, W. H. & JOUBERT, P. 1969 Rough wall turbulent boundary layer. *J. Fluid Mech.* **165**, 163–199.

- RAUPACH, M. R., ANTONIA, R. A. & RAJAGOPALAN, S. 1991 Rough-wall turbulent boundary layers. *Appl. Mech. Rev.* **44**, 1–25.
- SCHLICHTING, H. 1979 *Boundary-Layer Theory*, 7th edn. McGraw-Hill.
- SCHULTZ, M. P. & FLACK, K. A. 2007 The rough-wall turbulent boundary layer from the hydraulically smooth to the fully rough regime. *J. Fluid Mech.* **580**, 381–405.
- SHOCKLING, M. A., ALLEN, J. J. & SMITS, A. J. 2006 Roughness effects in turbulent pipe flow. *J. Fluid Mech.* **564**, 267–285.
- TOWNSEND, A. A. 1976 *The Structure of Turbulent Shear Flow*, 2nd edn. Cambridge University Press.
- VOLINO, R. J., SCHULTZ, M. P. & FLACK, K. A. 2007 Turbulence structure in rough- and smooth-wall boundary layers. *J. Fluid Mech.* **592**, 263–293.
- VOLINO, R. J., SCHULTZ, M. P. & FLACK, K. A. 2009 Turbulence structure in a boundary layer with two-dimensional roughness. *J. Fluid Mech.* **635**, 75–101.
- WU, Y. & CHRISTENSEN, K. T. 2007 Outer-layer similarity in the presence of a practical rough-wall topography. *Phys. Fluids* **19**, 085108.
- ZHOU, J., ADRIAN, R. J., BALACHANDAR, S. & KENDALL, T. M. 1999 Mechanisms for generating coherent packets of hairpin vortices in channel flow. *J. Fluid Mech.* **387**, 353–396.